LAWRENCE
LIVERMORE
NATIONAL
LABORATORY

UCRL-CONF-224597

MODELING AND THE SPUTTER DEPOSITION OF COATINGS ONTO SPHERICAL CAPSULES

A. F. Jankowski, J. P. Hayes

September 21, 2006

International Conference on Metallurgical Coatings and Thin Films
San Diego, CA, United States
April 23, 2007 through April 27, 2007

Modeling and the sputter deposition of coatings onto spherical capsules

Alan F. Jankowski and Jeffrey P. Hayes

Lawrence Livermore National Laboratory
Chemistry, Materials, and Life Sciences Department
P.O. Box 808, MS L-352, Livermore, CA 94550

ABSTRACT

The sputter deposition of coatings onto capsules of polymer and oxide shells as well as solid metal spheres is accomplished using a chambered substrate platform. Oxides and metal coatings are sputter deposited through a screen-aperture array onto a 0.3-1.2 mm diameter, solid spheres and hollow shells. Each shell is contained within its own individual chamber within a larger array. Ultrasonic vibration is the method used to produce a random bounce of each capsule within each chamber, in order to produce a coating with uniform thickness. Characterization of thin aluminum-oxide coated, platinum solid spheres and thicker copper-gold layer coated, hollow capsules (of both glass and polymer) show that uniform coatings can be produced using a screen-aperture chambered, substrate platform. Potential advantages of this approach compared to open-bounce pans include improved sample yield and reduced surface roughness from debris minimization. A process model for the coating growth on the capsules is developed to assess selection of the screen aperture based on the effects of sputter deposition parameters and the coating materials.

KEY WORDS: *sputtering; deposition process; growth mechanism*

INTRODUCTION

There are numerous applications for coating capsules and spheres. These include uses as low-friction hard coatings for bearings, resistance to corrosive and high-temperature conditions, and as

pressure vessels. In the later application, the coatings are ablative in the form of a pressure vessel designed to contain hydrogen as a gas, liquid, or frozen as a solid.[1-3] The ablative coating is typically deposited onto a capsule that is hollow consisting of a thin-walled polymer or glass shell. In typical deposition processes, the coating is applied as the capsule bounces in an open-pan configuration.[4-5] The capsule bounce motion is considered random as, in general, a uniform coating thickness is found in cross-section images of the capsule. Typically, the bounce is mechanically induced by a piezoelectric driven transducer that controls the lateral and transverse motions to the pan. Difficulties do arise when the capsule mass and diameter change, thereby requiring a continuous tuning of the bounce pan. Additionally, the coating material itself may influence the static charge collected by the capsule, hence the tendency to cluster together from an open configuration. Also, the cyclic nature of the piezoelectric can produce null as well as run-away modes of motion, i.e. very small or large amplitudes of displaced motion. Thus, it is desirable to have each capsule move with similar well-defined boundary conditions. Improvement in controlling capsule motion will further improve sample yield and thickness uniformity.

Previously [6], the coating of capsule shell was assessed using individual chambers with a volume several times the size of the capsule diameter. Several potential advantages to chambering each capsule with an aperture were identified in comparison to the conventional open-bounce pan configuration to reduce coarsening of the columnar coating, hence the surface roughness. One advantage is by minimizing glancing angles of deposition on the capsule, the most significant of which occur at the equator. A second is to minimize an uncontrolled heating of the capsule surface that may result from full exposure to the deposition source plasma. A third advantage is to minimize exposure of the capsule surface to particulate debris that often accumulates in the bounce pan configuration. In addition, a chambered capsule confines run-away motion as is induced in the bounce-pan configuration with piezoelectric-drive thermal cycles.

Two different material systems will be evaluated in this study: a submicron thin coating of alumina (Al-oxide) onto solid platinum (Pt) spheres; and a laminate coating of gold-copper (Au-Cu)

onto hollow silica capsules. A model is concurrently developed to predictive determine the coating thickness as based on selection of screen aperture dimensions and the deposition rate as calibrated to deposits on stationary flats.

EXPERIMENTAL

The substrates are coated by sputter deposition through a screen aperture into individual substrate chambers as shown in the Fig. 1 schematic. The substrates are configured as to provide random motion of each capsule within its own chamber. The ultrasonic vibration configuration seen in the Fig. 2 photograph features a piezoelectric that is driven at high frequency to create a surface wave in the substrate base platform that translates vertically to displace the capsule. The piezoelectric is mounted on a water-cooled copper platen to stabilize its operating temperature. The substrates for the Al-oxide coating are 0.3-0.6 mm diameter solid Pt spheres. Four different screens are used as listed in Table 1. For the Au-Cu coating, the substrates are 0.4-1.2 mm diameter polymer and silica glass shells that have a wall thickness less than 10 μm. A stationary silica-glass slide is used for thickness calibration measurements in both cases. The sputter deposition of the coatings utilizes a coating system that features an array of planar magnetrons with 3.3-7.6 cm diameter targets. For these experiments, the magnetron sources are operated at a forward power of 15-150 W with a discharge of 305-430 V using a 28-35 $cm^3 \cdot m^{-1}$ flow of argon (Ar) at a 1.3-2 Pa working gas pressure. The base pressure of the vacuum chamber is 5×10^{-6} Pa. The sources are positioned 5.7-8.9 cm above the substrates. The resonant frequency and amplitude of the ultrasonic drive are tuned to mobilize the substrates. For example, a 29.0 kHz frequency with a 20.2-20.6 V drive amplitude mobilizes the solid metal spheres. Measurements of coating thickness are made using contact profilometry. Imaging of some samples is accomplished using scanning electron microscopy (SEM) after preparing cross-sections by focused ion-beam (FIB) milling.

MODEL

By conservation of mass, the deposition from the source arriving at the screen mask is reduced in two steps: first, by deposition onto the top surface of the screen; and second, by deposition onto the aperture walls. To address the first step of reduction, the average thickness ($\boldsymbol{\ell}_{ave}$) of the coating that is deposited relative to the maximum thickness ($\boldsymbol{\ell}_{max}$) of the coating without the screen mask is proportional to the screen porosity ($\boldsymbol{p}$), as given by the relationship

$$\boldsymbol{\ell}_{ave} = \boldsymbol{p}\cdot\boldsymbol{\ell}_{max} \tag{1}$$

In eqn. (1), the thickness of the mask is not considered. The fractional porosity ($\boldsymbol{p}$) of the screen relative to 1, is given by the relationship

$$\boldsymbol{p} = 1-(\boldsymbol{\rho}_s\cdot\boldsymbol{\rho}_{sm}^{-1}) \tag{2}$$

where $\boldsymbol{\rho}_s$ is the density of the screen and $\boldsymbol{\rho}_{sm}$ is the density of the screen material. ($\boldsymbol{\rho}_{sm}$ equals 7.9 gm·cm^{-3} for the steel that is selected for use in this study.) In the second step of reduction, the diffusive scattering of the sputtered atoms coats the aperture side walls. In this second step, the screen thickness is accounted for. Each aperture in the screen is statistically assumed to be identical in height ($\boldsymbol{h}$) and width diameter ($\boldsymbol{w}$) of the hole. For ***each*** aperture, the amount that enters the aperture is equal to the volume that exits plus the amount that coats the aperture sidewall. This equality is expressed as

$$\boldsymbol{\ell}_{ap}\cdot(0.25\cdot\pi\cdot\boldsymbol{w}^2) = \boldsymbol{\ell}\cdot(0.25\cdot\pi\cdot\boldsymbol{w}^2)+ \boldsymbol{\ell}_w\cdot(\pi\cdot\boldsymbol{w}\cdot\boldsymbol{h}) \tag{3}$$

where $0.25\cdot\pi\cdot\boldsymbol{w}^2$ is the area of the aperture, $\pi\cdot\boldsymbol{w}\cdot\boldsymbol{h}$ is the area of the sidewall, $\boldsymbol{\ell}_{ap}$ is coating thickness that enters each aperture, $\boldsymbol{\ell}$ is coating thickness that exits the aperture, and $\boldsymbol{\ell}_w$ is coating thickness on the aperture wall. Introducing an aperture coefficient ($\boldsymbol{c}_a$) to relate the proportion of coating that coats the aperture wall to that which exits, according to the expression

$$\boldsymbol{\ell}_w = \boldsymbol{c}_a\cdot\boldsymbol{\ell} \tag{4}$$

eqn. (3) can then be rewritten as

$$\boldsymbol{\ell} = \boldsymbol{\ell}_{ap}\cdot[1+ \boldsymbol{c}_a\cdot(4\boldsymbol{h}\cdot\boldsymbol{w}^{-1})]^{-1} \tag{5}$$

Next, consider the specific case for coating capsules that randomly move beneath the screen aperture within each chamber. By combining the effects of aperture thickness with screen porosity, the value for $\boldsymbol{\ell}_{ap}$ in eqn. (5) equates to $\boldsymbol{\ell}_{ave}$ of eqn. (1). Thus, introducing eqn. (1) into (5), eqn. (5) can be rewritten as

$$\boldsymbol{\ell}_b = \boldsymbol{p}\cdot\boldsymbol{\ell}_{max}\cdot[1+ \boldsymbol{c}_a\cdot(4\boldsymbol{h}\cdot\boldsymbol{w}^{-1})]^{-1} \qquad (6)$$

where $\boldsymbol{\ell}_b$ is now the ***average*** coating thickness distributed over the base of the screen apertured chamber. The coating thickness ($\boldsymbol{\ell}_s$) that results on a capsule is determined by considering the ratio of the cross-section area ($\boldsymbol{A}_c$) versus its surface area ($\boldsymbol{A}_s$), according to the volume equivalence expression

$$\boldsymbol{\ell}\cdot\boldsymbol{A}_c = \boldsymbol{\ell}_s\cdot\boldsymbol{A}_s \qquad (7)$$

For a spherical capsule of diameter $\boldsymbol{d}$, the cross-section area $\boldsymbol{A}_c$ is $0.25\cdot\pi\cdot\boldsymbol{d}^2$ and the surface area $\boldsymbol{A}_s$ is $\pi\cdot\boldsymbol{d}^2$. Therefore, introducing eqn. (7) into (6), eqn. (6) for a spherical capsule is rewritten as

$$\boldsymbol{\ell}_s = 0.25\cdot\boldsymbol{p}\cdot\boldsymbol{\ell}_{max}\cdot[1+ \boldsymbol{c}_a\cdot(4\boldsymbol{h}\cdot\boldsymbol{w}^{-1})]^{-1} \qquad (8)$$

where $\boldsymbol{\ell}_s$ is the coating thickness on the capsule, $\boldsymbol{p}$ is the porosity of the screen mask, $\boldsymbol{h}$ is the height of the aperture (i.e. the screen thickness), $\boldsymbol{w}$ is the aperture width (i.e. the diameter of each hole in the screen), and $\boldsymbol{c}_a$ is an aperture coefficient that accounts for some percentage of coating on the aperture walls.

These geometric expressions are modeled to account for the mass transport from the target to the substrate during the deposition process. This capability enables a predictive determination of deposition rate as based on rate calibrations using a stationary substrate flat positioned beneath the screen mask. In this way, the efficiency of using screens with various hole sizes, porosity, and thickness can be evaluated. The aperture coefficient ($\boldsymbol{c}_a$) can be obtained from such calibration measurements on ***stationary*** flats (where $\boldsymbol{\ell}_{ap}$ equals $\boldsymbol{\ell}_{max}$) by rewriting eqn. (5) as

$$\boldsymbol{c}_a = [(\boldsymbol{\ell}_{ap}\cdot\boldsymbol{\ell}^{-1})\text{-}1]\cdot\boldsymbol{w}\cdot(4\boldsymbol{h})^{-1} \qquad (9)$$

An expression for the deposition rate ($\boldsymbol{r}_s$) onto a sphere directly follows from eqn. (8) as

$$r_s = \ell_{max} \cdot p \cdot [1 + c_a \cdot (4h \cdot w^{-1})]^{-1} \cdot (4t)^{-1} \quad (10)$$

where the time (t) of the deposition process is taken into account. The expression for the deposition rate (r_s) in eqn. (10) can be rewritten as

$$r_s = \ell_{max} \cdot c_s \cdot (4t)^{-1} \quad (11)$$

where the screen coefficient (c_s) is defined as

$$c_s = p \cdot [1 + c_a \cdot (4h \cdot w^{-1})]^{-1} \quad (12)$$

By introducing eqn. (5) into (12), and considering that ℓ_{ap} equals ℓ_{max} for stationary flats, c_s can be written as

$$c_s = p \cdot \ell \cdot (\ell_{max})^{-1} \quad (13)$$

An expression for ℓ_s as a function of c_s is derived by introducing eqn. (12) into (8) and can be written as

$$\ell_s = 0.25 \cdot c_s \cdot \ell_{max} \quad (14)$$

RESULTS AND ANALYSIS

Results are given in Table 1 for the evaluation of four different screen apertures used during the deposition of an rf-sputtered Al-oxide coating of 4.10±0.11 μm thickness (ℓ_{max}) over a time interval (t) of $1.41 \cdot 10^3$ m. A 7.6 cm diameter planar magnetron with an alumina target was operated at 150 W forward power in the rf mode at a 8.9 cm source-to-substrate separation (z) using a 2 Pa Ar gas pressure and 35 $cm^3 \cdot s^{-1}$ flow. The values listed in Table 1 are computed as follows: p from eqn. (2); c_a from eqn. (9); c_s from eqn. (13); and r_s from eqn. (11). Note that computed r_s values are listed in units of $nm \cdot kW^{-1} \cdot m^{-1}$ after normalization to the forward target power. Thus, the computed r_s values can be compared to a maximum stationary rate of 19.4±0.5 $nm \cdot kW^{-1} \cdot m^{-1}$ on an unmasked silica flat. For the maximum r_s condition produced with screen no. 1, only 4.8% of the stationary rate would transferred onto the moving capsule surface. In comparing the different screen apertures for the data of this Al-oxide deposition listed in Table 1, the r_s varies linearly with c_s according to the following expression

$$r_s = 4.8952 \cdot c_s - 0.0072 \qquad (15)$$

where the correlation coefficient (R^2) of the linear regression analysis equals 0.9997. The relationship of eqn. (15) is evident through examination of eqn.(12), as the coating throughput for each screen are related geometrically to the (gas pressure, source-to-substrate separation, etc.) conditions for this sputter deposition.

In Table 2, a additional data set is listed using screen no. 3 for the deposition of an Al-oxide coating that is three times as thick onto a stationary flat. The 14.6 μm coating (as deposited onto a stationary witness slide of fused silica) was processed using a 3.3 cm diameter planar magnetron operated again at 2 Pa Ar gas pressure and 35 $cm^3 \cdot s^{-1}$ flow in the rf mode but with a 70 W forward power setting and only a 5.1 cm source-to-substrate separation. The use of screen no.3 provides a thicker mask that is less likely to distort than the other screens under the thick coating applied. Although screen no. 3 has the lowest porosity, it has the second highest rate (as listed in Table 1) attributable to the largest $w:h$ ratio of 1.35±0.07 for the four screens considered in this study. The aperture c_a and screen c_s coefficients obtained from this second screen no. 3 coating are nearly identical to those values obtained using the 7.6 cm diameter magnetron in the first screen no. 3 Al-oxide deposition. The consistency between deposition experiments helps validate the present model for a sputtered species through a screen aperture onto a capsule.

In general, higher throughput onto the capsule occurs as c_a decreases whereas the magnitude of c_s increases. These coefficients would be expected to change with variation of the gas pressure. A change in pressure causes a variation in the scattering of the sputtered neutrals. The c_a value should increase whereas c_s would decrease with an increase in pressure as the scattering of sputtered neutrals becomes more diffuse. The coating thickness (ℓ_s) on the sphere listed in Table 2 is computed using eqn. (14). The measured coating thickness (ℓ_s^m) provides a comparison to those samples imaged in cross-section using scanning electron microscopy. Whereas the Al-oxide coated Pt spheres were not imaged in

cross-section, a masked surface region of one 0.6mm diameter Pt sphere was profiled. A step height of 0.54±0.05 μm was measured between coated and uncoated regions using contact profilometry. The computed and measured values are in agreement within experimental error.

Screen no. 3 was selected as well for use in depositing a Au-Cu coating onto hollow polymer and silica glass capsules. The silica capsules have a wall thickness of only 4 μm. The laminate coating consists of a Cu on Au layer pair. The Au layer is first deposited in 390 m using a 3.3 cm diameter planar magnetron operated in the dc mode with 1.3 Pa Ar gas pressure and 28 $cm^3 \cdot s^{-1}$ flow at a 30 W forward power setting and only a 5.7 cm vertical source-to-substrate separation. The Cu layer is next deposited in 1100 m using a 15 W forward power setting. Thickness measurements are listed in Table 2 as taken from different masked regions of stationary witness slides positioned at different distances from the centerline of the magnetron source. The coating thickness and deposition rate increase from the perimeter to the centerline as seen in the tabulated data for both Au and Cu. Results are tabulated as well for a submicron thin deposit of titanium (Ti). The Ti was deposited in 72 m using a 30 W forward power (and the same gas pressure and source-to-substrate separation as used for both the Au and Cu depositions).

The $\boldsymbol{c}_s$ values remain constant for each material as expected. From the Table 2 data, it's seen that the screen coefficient ($\boldsymbol{c}_s$) value varies ***between*** the materials being deposited for screen no. 3 (as it will with each screen aperture). The value for $\boldsymbol{c}_s$ appears trend increase with the density of the sputtered species. The $\boldsymbol{c}_s$ values trend increase with the density of the materials being deposited as the heavier metals scatter less providing a greater line-of-sight to the substrate. The variation of the screen coefficient ($\boldsymbol{c}_s$) with material density ($\boldsymbol{\rho}_m$) is best fit a natural logarithmic function according to the following expression

$$\boldsymbol{c}_s = 0.0682 \cdot \ln(\boldsymbol{\rho}_m) + 0.0759 \qquad (16)$$

where the correlation coefficient (R^2) of the logarithmic regression analysis equals 0.9844. This result correlates with the logarithmic relationship observed between mean free path (and arriving sputter rate) with mass (or material density) as related to the sputter yield, working gas pressure, and gas scattering effects [7-8].

The model calculation for ℓ_s is in general agreement with the measured ℓ_s^m values of Table 2 across a wide range of deposition rates and coating thickness (ℓ) values. (The ℓ_s values may trend higher than ℓ_s^m as the witness measurement is made from a position at the edge of the selected chambered capsule, i.e. slightly further away from the magnetron center and thus at a slightly lower rate.) A SEM image of a FIB cross-section is shown in Fig. 3 for the coated capsule sample from the deposition where $\ell^{Cu}{}_{max}$ equals 41.9 μm and $\ell^{Au}{}_{max}$ equals 35.5 μm. A low magnification (Fig. 4) image shows several Au-Cu coated capsules in full. Energy dispersive x-ray analysis confirms the elemental composition of each constituent layer. Vicker microhardness measurements from the cross-section indicate the Au layer has a 0.93±0.04 GPa hardness and the Cu layer a 2.10±0.07 GPa hardness.

SUMMARY

A process model for coating-thickness growth on capsules is developed to assess selection of the screen aperture based on the effects of sputter deposition parameters and the coating materials. The sputter deposition of coatings onto capsule surfaces is considered [6] through use of an ultrasonic drive and a chambered configuration (of Figs. 1-2). A single aperture is now replaced with a screen (in Fig. 1) wherein the width and depth of each opening are assessed to provide a predictive determination of the coating thickness. An aperture coefficient (c_a) for each screen is determined through eqn. (9) from rate calibration experiments onto stationary substrates listed in Table 1. A screen coefficient (c_s) derived from c_a through eqn. (12) provides a subsequent direct link to predict coating thickness (ℓ_s) on each chambered capsule through eqn. (14). The deposition rate (r_s) of a single material for each unique

deposition condition experiment is found to be directly proportional to the screen coefficient (c_s) as seen in eqn. (15). For different coating materials listed in Table 2, the screen coefficient is logarithmically proportional to the material density as seen in eqn. (16). In assessing the feasibility of applying this deposition method to produce a Cu-on-Au layered coating design [3], the predicted coating thickness (ℓ_s) values are within the error range of the measured coating thickness (ℓ_s^m) as shown in Fig. 3.

ACKNOWLEDGEMENTS

The authors thank N. Teslich and J. Ferreira for their assistance in the focused-ion beam sectioning and scanning electron microscopy imaging and composition analysis. This work was performed under the auspices of the U.S. Department of Energy by the University of California, Lawrence Livermore National Laboratory under contract No. W-7405-Eng-48.

REFERENCES

1. J.A. Paisner, J.D. Boyes, S.A. Kumpan et al., Laser Focus World 30 (1994) 75.

2. S.W. Haan, S.M. Pollaine, J.D. Lindl et al., Phys. Plasmas, 2 (1995) 2480.

3. P. Amendt, J.D. Colvin, R.E. Tipton, et al., Phys. Plasmas, 9 (2002) 2221.

4. S. Meyer, E. Hsieh, and R. Burt, Thin Solid Films, 72 (1980) 375.

5. A. Nikroo and D. Woodhouse, Fusion Technol., 35 (1999) 202.

6. A.F. Jankowski, J.P. Hayes, and J.D. Morse, Thin Solid Films 398/399 (2001) 587.

7. W.D. Westwood, J. Vac. Sci. Technol. 15 (1978) 1.

8. R.E. Somekh, J. Vac. Sci. Technol. A 2 (1984) 1285.

Table 1. Deposition of the 4.1 μm thick Al-oxide coating through four screen apertures							
Screen	h (μm)	w (μm)	p	ℓ (μm)	c_a	c_s	r_s (nm·kW^{-1}·m^{-1})
1	130±1	155±25	0.356±0.002	2.21±0.02	0.256±0.065	0.192±0.007	0.933±0.022
2	360±3	380±10	0.348±0.002	1.83±0.08	0.327±0.057	0.155±0.008	0.753±0.018
3	360±3	485±25	0.289±0.001	2.40±0.01	0.239±0.033	0.169±0.005	0.820±0.021
4	200±2	225±25	0.395±0.003	1.68±0.03	0.405±0.085	0.162±0.007	0.784±0.022

Table 2. Variation of c_a and c_s coefficients with sputter condition and materials using screen no. 3							
Material	ℓ_{max} (μm)	ℓ (μm)	c_a	c_s	r_s (nm·kW^{-1}·m^{-1})	ℓ_s (μm)	ℓ_s^m (μm)
Al-oxide	4.10±0.11	2.40±0.01	0.239±0.033	0.169±0.005	0.82±0.02	0.17±0.01	-
Al-oxide	14.6±0.3	8.1±0.5	0.270±0.073	0.160±0.013	1.20±0.13	0.58±0.06	0.54±0.05
Ti	0.81±0.02	0.52±0.02	0.187±0.048	0.186±0.012	0.017±0.002	0.038±0.003	0.06±0.01
Cu	22.3±0.5	17.8±0.2	0.085±0.021	0.231±0.005	78.1±3.4	1.29±0.06	1.51±0.06
Cu	41.9±1.3	33.0±0.5	0.091±0.027	0.228±0.010	145±11	2.39±0.18	2.69±0.12
Au	18.8±0.1	18.0±0.1	0.015±0.005	0.277±0.003	111±2	1.30±0.02	1.43±0.08
Au	35.5±0.4	33.7±0.2	0.018±0.008	0.274±0.005	208±6	2.43±0.07	2.61±0.04

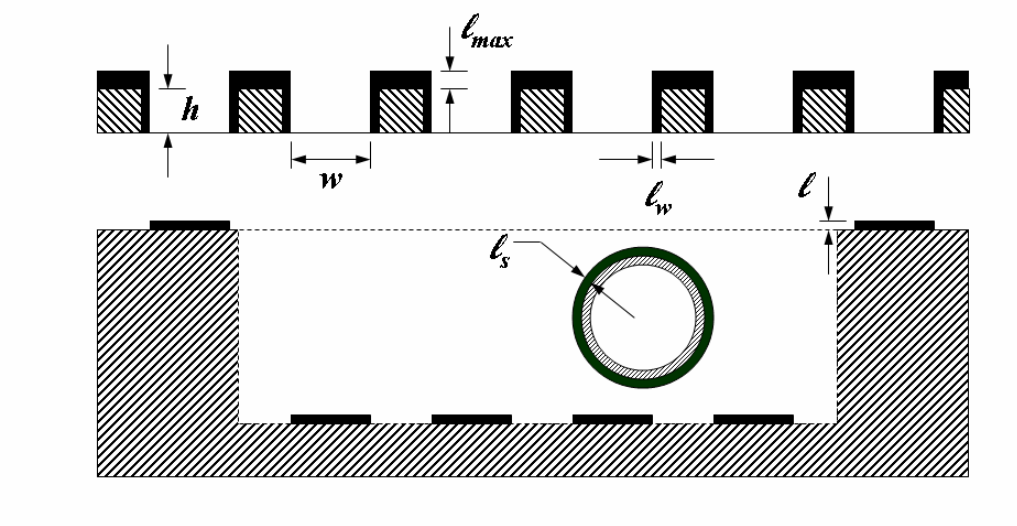

Figure 1. A schematic of the screen-aperture chamber is shown in which each capsule is sputter coated while randomly moving as driven by ultrasonic vibration. The width (w) and height (h) of each aperture are labeled as is the coating thickness on the capsule surface (ℓ_s), after exiting the aperture (ℓ), on the aperture wall (ℓ_w), and at its maximum value on the screen aperture entrance surface (ℓ_{max}).

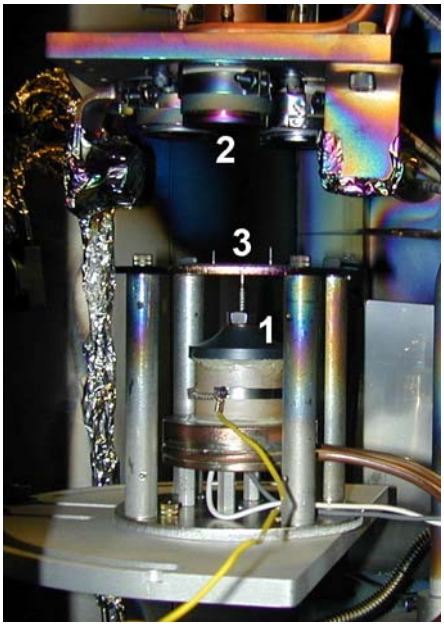

Figure 2. The screen aperture over the chambered bounce pan is driven by a piezoelectric transducer (1). The array of planar magnetron sources (2) is situated above the chambered substrate platform (3).

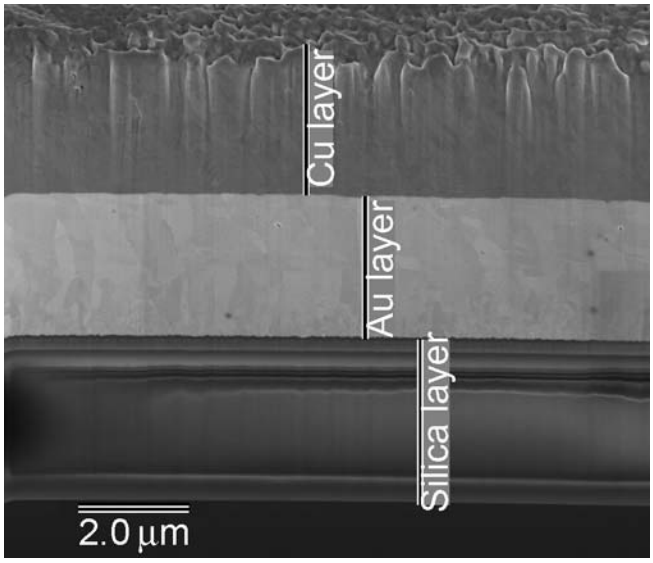

Figure 3. The scanning electron microscope image is shown of the Cu-on-Au bilayer coated, silica capsule as cross-sectioned using a focused ion beam.

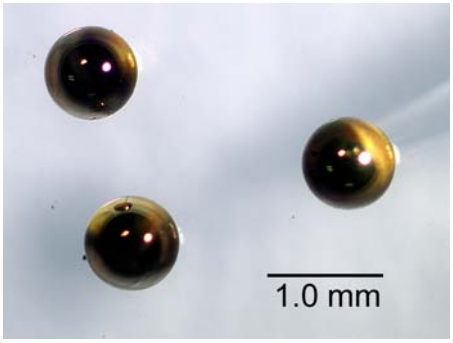

Figure 4. Three coated capsules are shown in the low-magnification optical photomicrograph.